High-spin proton alignments and coexisting coupling schemes in ^{168}Hf

R. B. Yadav,[1] W. C. Ma,[1] G. B. Hagemann,[2] H. Amro,[1] A. Bracco,[3] M. P. Carpenter,[4] J. Domscheit,[5] S. Frattini,[3] D. J. Hartley,[6] B. Herskind,[2] H. Hübel,[5] R. V. F. Janssens,[4] T. L. Khoo,[4] F. G. Kondev,[7] T. Lauritsen,[4] C. J. Lister,[4] B. Million,[3] S. Ødegård,[8] L. L. Riedinger,[9] K. A. Schmidt,[2] S. Siem,[8] G. Sletten,[2] P. G. Varmette,[1,2] J. N. Wilson,[2] and Y. C. Zhang[1]

[1]*Department of Physics, Mississippi State University, Mississippi State, Mississippi 39762, USA*
[2]*The Niels Bohr Institute, Blegdamsvej 17, DK-2100 Copenhagen, Denmark*
[3]*Dipartimento di Fisica, Università di Milano, Via Celoria 16, I-20133 Milano, Italy*
[4]*Physics Division, Argonne National Laboratory, Argonne, Illinois 60439, USA*
[5]*Helmholtz-Institut für Strahlen- und Kernphysik, University of Bonn, D-53115 Bonn, Germany*
[6]*Department of Physics, United States Naval Academy, Annapolis, Maryland 21402, USA*
[7]*Nuclear Engineering Division, Argonne National Laboratory, Argonne, Illinois 60439, USA*
[8]*Department of Physics, University of Oslo, N-0316 Oslo, Norway*
[9]*Department of Physics and Astronomy, University of Tennessee, Knoxville, Tennessee 37996, USA*

(Received 28 September 2009; published 7 December 2009)

High-spin states in ^{168}Hf were populated in the ^{96}Zr(^{76}Ge,4n) reaction and the decay γ rays measured with the Gammasphere spectrometer array. Previously known bands were extended to significantly higher spins and seven new bands were established. The results were interpreted within the framework of the cranked shell model with the help of comparisons with neighboring nuclei. The observation of full alignment in band crossings at a rotational frequency $\hbar\omega \sim 0.55$ MeV revealed that these crossings are associated with proton alignments involving $h_{11/2}$ and $h_{9/2}$ orbitals. The characteristics of one strongly coupled high-K band indicate that the deformation-aligned configuration is built on the same six quasiparticles that constitute the high-spin structure of a rotationally aligned band. This leads to the coexistence of two coupling schemes, deformation and rotation alignment, in six-quasiparticle structures involving the same orbitals.

DOI: 10.1103/PhysRevC.80.064306 PACS number(s): 21.10.Re, 23.20.Lv, 25.70.−z, 27.70.+q

I. INTRODUCTION

The search for experimental signatures of triaxial nuclear shapes in the mass $A \sim 160$ region has drawn considerable interest in recent years. Indeed, high-spin triaxial strongly deformed (TSD) structures have been identified in several Lu ($Z = 71$) isotopes, and the wobbling motion, a low-lying collective excitation mode characteristic of nuclei with stable triaxiality [1], has been identified in ^{163,165,167}Lu [2–5] and possibly in $^{161}_{71}$Lu [6]. An extensive search for TSD bands in Hf ($Z = 72$) nuclei has also been carried out, and a number of strongly deformed bands have been observed in ^{170}Hf [7], ^{171,172}Hf [8], ^{173,174}Hf [9,10], and ^{175}Hf [11]. The rotational properties of these bands were studied systematically and compared with cranking calculations using the ULTIMATE CRANKER (UC) code [12,13] and in the framework of cranked relativistic mean-field (CRMF) calculations. As a result, the bands were suggested to fall into two groups, labeled as ED and SD. The ED bands are likely built on the proton $i_{13/2}h_{9/2}$ configuration, associated with near prolate shapes and deformations ($\varepsilon_2 \sim 0.3$) enhanced relative to the normal deformed (ND) nuclear shapes ($\varepsilon_2 \sim 0.22$) characterizing the respective ground states. The SD bands are likely associated with superdeformed prolate shapes with little triaxiality. For example, the measured quadrupole moments are $Q_t \sim 12.6$–13.8 e b for these bands in $^{173-175}$Hf [10,11]. The SD structures involve the $\pi i_{13/2}$ (proton), as well as the $\nu j_{15/2}$ (neutron) orbitals originating from above the $N = 126$ spherical shell closure [8].

Three candidate TSD bands were reported in ^{168}Hf [14], and the measured moment $Q_t \sim 11.4\,e$ b for Band TSD1 is close to the UC predicted value for a TSD band. In a later study of the possible decay pathways associated with these bands [15], the spin and excitation energy of the strongest band, TSD1, were approximately determined based on γ-ray coincidence relationships. Discrete links were established for the second band. The overall agreement between the observed properties of the bands and UC calculations provides strong support for an interpretation where the TSD1 band is associated with a TSD minimum, $(\varepsilon_2, \gamma) \sim (0.43, 20^\circ)$, involving the $\pi(i_{13/2})^2$ and the $\nu(j_{15/2})$ high-j orbitals. This constitutes the first identification of a TSD band in Hf isotopes. The second band is understood to be another ED band, similar to those observed systematically in neighboring, heavier Hf isotopes. It is proposed to be built on the $\pi(i_{13/2}h_{9/2}) \otimes \nu(i_{13/2})^2$ configuration.

An extensive study of the ND level structures of ^{168}Hf has also been carried out and is the subject of this article. In fact, the study of the decay pathways from the TSD and ED bands to the ND levels became possible only after the ND structures were studied thoroughly. About 250 new transitions were placed in the level scheme. The six previously known bands [16] have now been extended to significantly higher spins. The proton alignment at a rotational frequency of $\hbar\omega \sim 0.55$ MeV can now be fully delineated and investigated. Seven new bands were identified, including three coupled bands, two of which are built on four quasiparticle (two protons and two neutrons) excitations. Interestingly, the third coupled band and one of

the previously known, and now extended, bands are proposed to involve the same orbitals. This observation is interpreted as a manifestation of the coexistence of the two different coupling schemes: deformation and rotation alignment. To our knowledge, such coexisting coupling schemes in six quasiparticle structures involving the same orbitals at high spins were previously reported only in ^{166}Hf [17]. High-spin band crossings and possible intrinsic configurations for each band were discussed based on the cranking calculations aided by a comparison with neighboring nuclei.

II. EXPERIMENT AND DATA ANALYSIS

Two experiments were performed using the reaction ^{96}Zr(^{76}Ge,4n) to populate high-spin states in ^{168}Hf. The details of the experiments are described in Ref. [14] and are briefly summarized here. The 310-MeV ^{76}Ge beam was provided by the ATLAS accelerator at Argonne National Laboratory. Coincident γ rays were measured using the Gammasphere array [18] that, at the time of the experiments, consisted of 101 Compton-suppressed Ge detectors. A self-supporting thin foil ($\sim$0.67 mg/cm^2) of isotopically enriched ^{96}Zr ("thin-target") was used as a target in the first experiment. A total of 2.2×10^9 five- and higher-fold prompt coincidence events was collected. In the second experiment, the target consisted of a thin layer of ^{96}Zr backed by 21 mg/cm^2 Au ("thick-target").

During the off-line analysis, the "thin-target" data were sorted into a database where the γ-ray energies and detector identification were stored for each event. The RADWARE software package [19] was used to construct three-dimensional (cube) and four-dimensional (hypercube) histograms and to analyze the γ-ray coincidence relationships. The "thick-target" experiment was mainly designed for lifetime measurements using the Doppler shift attenuation method (DSAM). The data were also used in the coincidence analysis for some low-spin transitions where the γ rays are fully stopped and the Doppler broadening is minimized.

Information about the multipolarity of the transitions was obtained from the analysis of so-called DCO ratios (γ-ray directional correlation from oriented nuclei [20]). Gated DCO matrices, with detectors at 31°, 37°, 143°, 148°, and 163° along the x axis, and detectors from 58° through 122° along the y axis, were constructed from the database for this purpose. The technique was calibrated with transitions of known multipolarity. The extracted DCO ratios from stretched quadrupole gated spectra fall into two distinct groups centered around 1.0 and 0.6 for stretched quadrupole and dipole transitions, respectively. The expected DCO ratios for various γ rays under different gating conditions are listed in Table I. The parity assignments are based on the multipolarities of γ-ray linking transitions, as well as coincidence relationships that may introduce important constraints. In some cases, the proposed configurations of the bands had to be used.

III. LEVEL SCHEME

The proposed level scheme for ^{168}Hf is presented in Fig. 1. The two TSD bands (not shown in the level scheme) and the ED band have been published previously [14,15] and will not be discussed in this article. Bands 1–6 were previously observed from a study using the reaction ^{124}Sn(^{48}Ti,4n) [16]. The β- and γ-vibrational bands were identified from β-decay experiments [21,22]. Seven new ND bands, Bands 7–13, have been identified, and many new interband transitions were established. Table AI (Appendix) lists the energies of the levels and γ rays, as well as the measured transition intensities and DCO ratios.

TABLE I. Expected DCO ratio of the second transition in a γ cascade, where the gate is set on the first transition. If the gate and the transitions are interchanged, the DCO ratio is inverted. Q and D refer to quadrupole and dipole transitions, respectively.

γ cascade					R_{DCO}
I	$\xrightarrow{Q}$	$I-2$	$\xrightarrow{Q}$	$I-4$	1.0
I	$\xrightarrow{Q}$	$I-2$	$\xrightarrow{D}$	$I-3$	$\sim$0.6
I	$\xrightarrow{Q}$	$I-2$	$\xrightarrow{D}$	$I-2$	$\sim$1.0
I	$\xrightarrow{Q}$	$I-2$	$\xrightarrow{Q}$	$I-2$	$\sim$0.6
I	$\xrightarrow{D}$	$I-1$	$\xrightarrow{D}$	$I-2$	1.0
I	$\xrightarrow{D}$	$I-1$	$\xrightarrow{D}$	$I-1$	$\sim$1.6

A. Bands 1–6

Band 1, previously observed up to 38^+ [16], has been extended to 48^+. It is the ground-state band and remains yrast after the alignment of the first pair of neutrons around spin 12^+ until Band 3 becomes yrast at 37^-. Band 2, the extension of the ground-state band, has been extended from 22^+ to 36^+. Six new linking transitions at 1012, 1323, 1357, 1386, 1429, and 1478 keV have been observed between the two bands. The measured DCO ratios for the 1357- and 1386-keV γ rays are consistent with an $E2$ character.

Bands 3 and 4, two negative-parity bands (identified as AE and AF bands in the previous work [16]), have been extended to 47^- and 40^-, respectively. A 7^- state was added as the lowest level in Band 3, together with a 978-keV depopulating transition from this level to Band 1. Five new $M1$ transitions, at 354, 332, 336, 347, and 356 keV, have been observed decaying from levels between 12^- and 20^- in Band 4 to levels in Band 3. All measured DCO ratios of decay-out transitions from these two bands agree with previous spin assignments [16]. The assigned negative parity came primarily from the proposed configuration of the bands. Coincidence spectra representative of Bands 1 and 3 are displayed in Fig. 2.

Band 5 (labeled as Band BE in the previous work [16]) has been extended from 24^- to 32^-. Seven new transitions have been observed decaying out from levels between 8^- and 20^- in Band 5 to levels in Band 3 and, in addition, another seven new transitions were observed from levels between 10^- and 22^- in Band 5 to levels in Band 4. A new 4^- level has been added at the bottom of Band 5, and two more decay-out transitions were placed that link the 10^- and 4^- states to levels in Band 1. Furthermore, two γ rays, at 263 and 427 keV, have been observed linking the 6^- level to $6^+$and 5^+ states of the

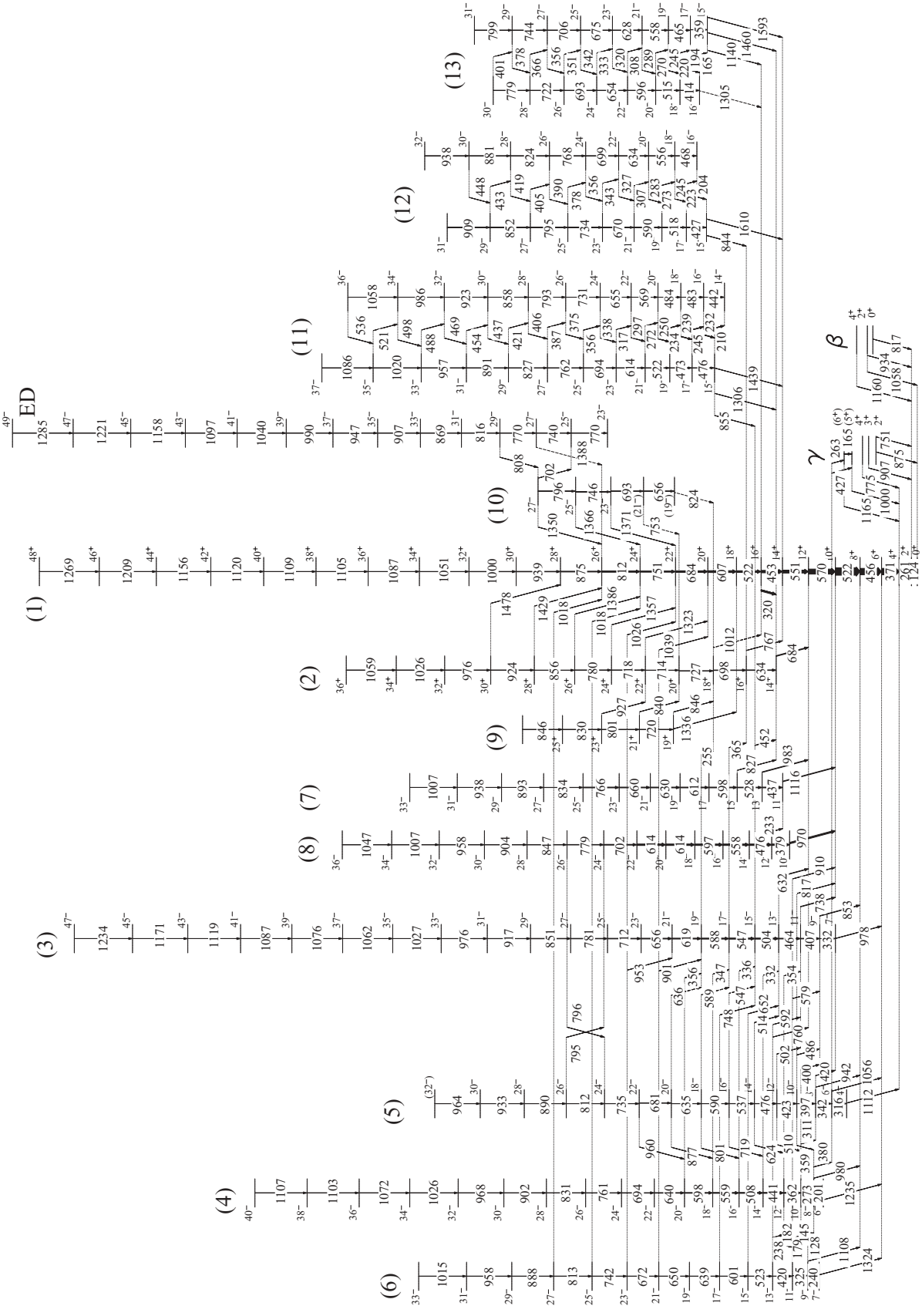

FIG. 1. Proposed level scheme for ^{168}Hf; arrow widths are proportional to the relative intensities of the γ rays. Energies are in keV. Two previously published TSD bands [14,15] are not shown in the level scheme.

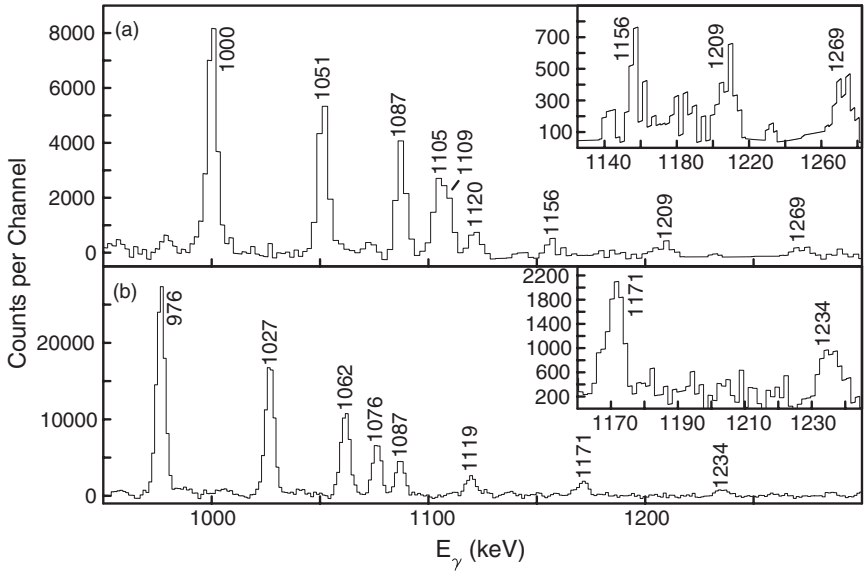

FIG. 2. Representative coincidence spectra for the high-spin regions of Bands 1 and 3. (a) Spectrum of Band 1 from a sum of double coincidence gates on transitions above level 24^+. (b) Spectrum of Band 3 from a sum of double gates on transitions above level 23^-. Insets display the highest-energy γ rays observed in the two bands.

γ band [21,22]. The measured multipolarities of all linking transitions agree with previous spin and parity assignments for Band 5.

Band 6 has been extended from 11^- to 33^-, with 11 new band members added [see Fig. 3(a)]. Three more $M1$ transitions have been found between low-spin levels in Bands 4 and 6. Four γ rays decay from levels between 11^- and 17^- in Band 6 to levels in Band 3. In addition, four transitions decay from levels between 21^- and 27^- directly to the yrast Band 1. All measured multipolarities of the 1324- and 1108-keV depopulation transitions from Band 6, of the intraband dipole transitions between Bands 4 and 6, and of the interband transitions to Band 1 support the previous spin and parity assignments for Band 6.

B. Bands 7–10

Band 7 consists of a cascade of 11 $E2$ transitions. The band decays directly to Band 1 through the 1116-, 983-, and 827-keV transitions. Measured DCO ratios indicate that the 1116- and

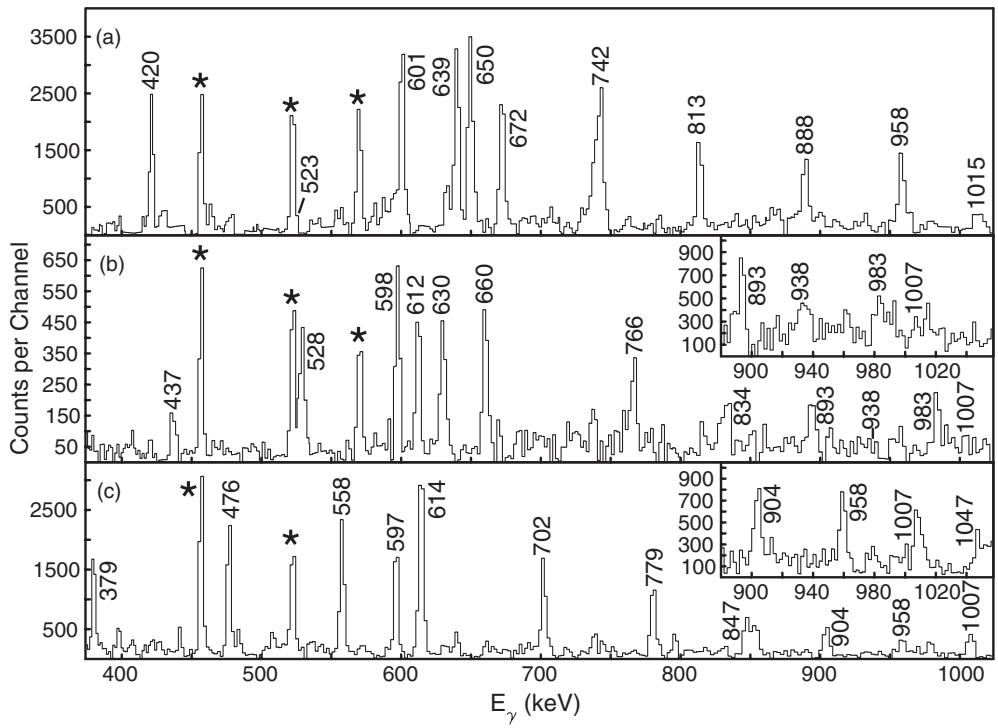

FIG. 3. (a) Spectrum of Band 6 from a sum of triple gates on transitions between levels 7^- and 29^-. (b) Spectrum of Band 7 from a sum of triple gates on transitions between levels 13^- and 27^-. The inset shows the high spin region of the band that is obtained by summing all triple coincidence spectra gated on transitions above the 19^- level. (c) Spectrum of Band 8 from a sum of triple gates on transitions between levels 10^- and 32^-. The inset shows the high-spin region of the band resulting from a sum of triple gates on transitions above the 24^- level.

983-keV transitions are stretched dipoles, thus resulting in odd spins for the states in this band. Band 8 consists of 13 members. A 233-keV $M1$ transition connects its 12^- level to the 11^- level in Band 7. The DCO ratio of the 970.4-keV γ ray connecting the lowest level of Band 8 and the yrast 10^+ level, is consistent with that of an unstretched ($\triangle I = 0$) dipole transition. Bands 7 and 8 are actually signature partners. This can be seen from their similar properties (see discussion in Sec. IV). Bands 7 and 8 are very weakly populated, with a total intensity of only $\sim$2.5% relative to the yrast band. This could be the reason for the observation of a single intraband transition, the 233-keV γ ray. Bands 8 and 5 interact at levels 24^- and 26^-, as shown by the two interband transitions (795 and 796 keV) decaying to each other. Therefore, Band 8 must have the same negative parity as Band 5. Band 7, as the signature partner of Band 8, must also be of the same negative parity. Double-gated spectra for Bands 7 and 8 are presented in Fig. 3.

Band 9 consists of a short sequence of four transitions. The measured DCO ratios for the two stronger transitions, at 720 and 801 keV, confirm their $E2$ nature. The DCO ratios of three depopulating transitions from Band 9 to Band 2 indicate that they are likely of the $M1/E2$ mixed type. Therefore, Band 9 has been assigned odd spins and positive parity.

Band 10 decays mainly to levels in Band 1 between 26^+ and 22^+ with the 1371-keV γ ray being the strongest linking transition. Band 10 also feeds Bands 2 and 3. However, the linking transitions to Band 3 could not be established. The 1371- and 1366-keV transitions depopulating Band 10 have DCO ratios of 0.49(9) and 0.69(10), respectively, consistent with a stretched dipole character. Furthermore, negative parity for Band 10 is proposed because the linking transitions most likely have an $E1$ multipolarity. An $M1$ transition of such high energy would be expected to exhibit an $E2$ admixture, resulting in a larger DCO ratio.

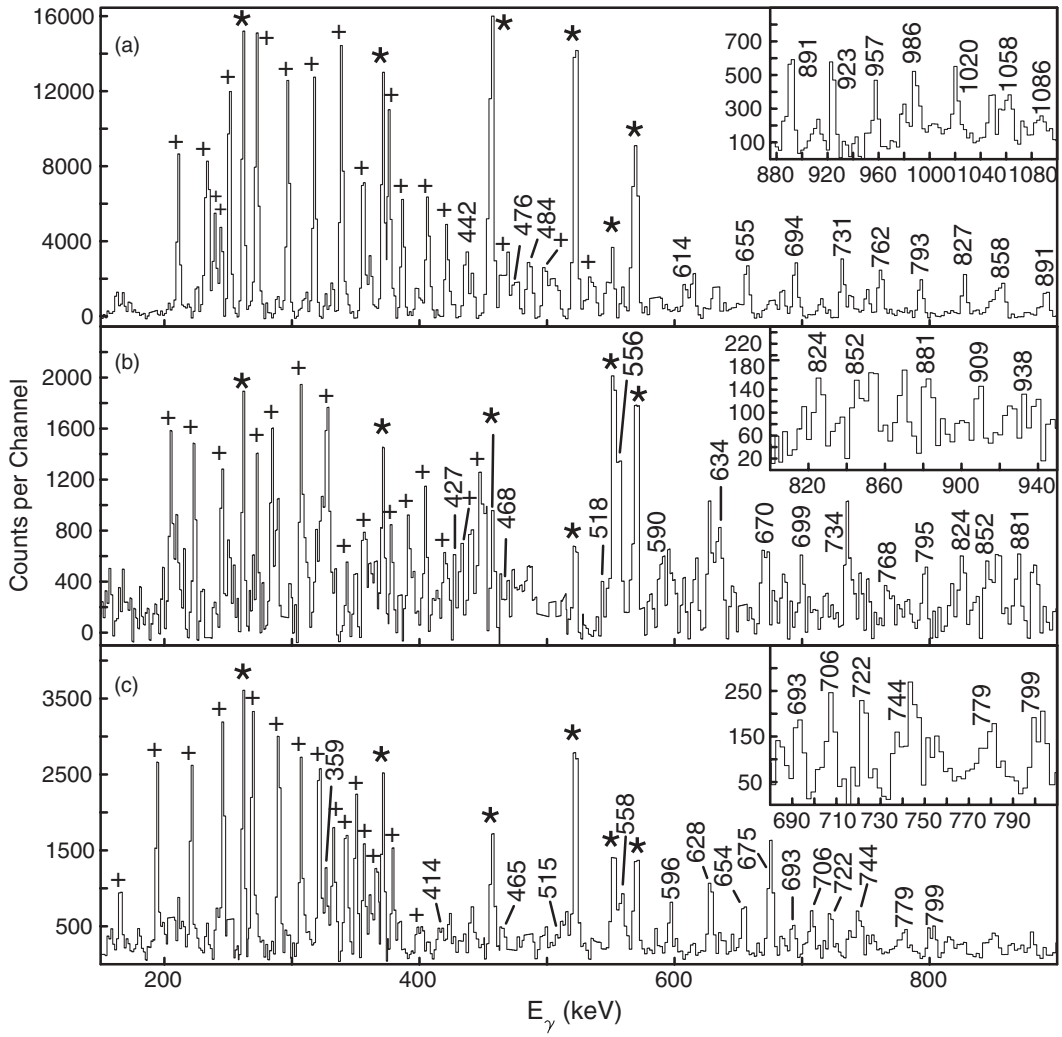

FIG. 4. (a) Spectrum of Band 11 from a sum of triple gates on $M1$ transitions between levels 14^- and 34^-. (b) Spectrum of Band 12 from a sum of triple gates on $M1$ transitions between levels 15^- and 29^-. (c) Spectrum of Band 13 from a sum of triple gates on $M1$ transitions between levels 15^- and 29^-. In each spectrum, the low-energy, high-intensity transitions are of $M1$ character and are marked with plus (+) signs; the higher-energy, lower-intensity transitions are of $E2$ multipolarity and are labeled by transition energies. The low-spin yrast transitions are marked by stars. The high-energy regions of the spectra are presented in the insets.

C. Bands 11–13

Three strongly coupled bands have been observed in ^{168}Hf for the first time. Their spectra are given in Fig. 4. Band 11 extends from 14^- to 37^-. Three interband linking transitions have been observed, with the two stronger ones depopulating the 15^- level and feeding the two 14^+ levels in Bands 1 and 2. A 855-keV γ ray decays from this 15^- level to 15^- state in Band 3. Band 12 extends from 15^- to 32^-. It decays to the 14^+ level in Band 1 and the 16^+ state in Band 2. Band 13 extends from 15^- to 31^-. It decays to the 14^+ state in Band 1 and the 14^+ and 16^+ levels in Band 2.

Measured DCO ratios of the stronger decay-out transitions from these three coupled bands (i.e., the 1306-keV γ ray from Band 11, the 844- and 1610-keV γ rays from Band 12, and the 1140-keV γ ray from Band 13) are all consistent with a stretched dipole nature. As mentioned above, such high-energy stretched dipole transitions are likely of the $E1$ type rather than the $M1$ one. Consequently, all three bands have been assigned negative parity. This is strongly supported by the configurations proposed for the bands in the next section.

IV. DISCUSSION

Cranking calculations for ^{168}Hf have been carried out with the UC code [12,13]. Proton and neutron orbital energies for the ND region are displayed on the Routhian diagrams in Fig. 5. Table II lists the labeling of the quasiparticles and related orbitals predicted by the UC code to be closest to the Fermi surface. Uppercase letters represent quasineutrons and lowercase letters quasiprotons. Each letter corresponds to a state described by a certain combination of asymptotic Nilsson orbitals and appropriate signature and parity quantum numbers. Corresponding shell model states are also listed in Table II. Configurations of the bands in ^{168}Hf are assigned below based on intrinsic properties of the bands, such as the observed alignments, crossings expected at specific frequencies, excitation energies, $B(M1)/B(E2)$ ratios for strongly coupled bands, and on a systematic comparison of these configurations with structures observed in neighboring nuclei. In Fig. 6 the experimental alignments of all bands, except for the two short Bands 9 and 10, are displayed as a function of rotational frequency. Harris parameters $J_0 = 25\hbar^2/\text{MeV}$ and $J_1 = 53\hbar^4/\text{MeV}^3$ were chosen such that Band 1 has zero initial alignment and Bands 3 and 4 (two-quasiparticle bands AE and AF) have a constant alignment above the first neutron (BC) crossing. The calculated and experimentally observed band crossings are summarized in Table III. Figure 7 provides the excitation energies of all bands in ^{168}Hf relative to a rigid-rotor reference $AI(I+1)$, where the inertia parameter A was chosen to be 7.8 keV.

TABLE II. Labels and alignments of theoretical Routhians.

Spherical shell models states	Nilsson orbitals	$\alpha = +1/2$		$\alpha = -1/2$	
		Label	i_x	Label	i_x
$\nu i_{13/2}$	$\nu[642]\frac{5}{2}^+$	A	5.5	B	4.5
$\nu i_{13/2}$	$\nu[651]\frac{3}{2}^+$	C	2.5	D	0.8
$\nu h_{9/2}$	$\nu[523]\frac{5}{2}^-$	E	1.8	F	1.5
$\nu f_{7/2}$	$\nu[521]\frac{3}{2}^-$	G	0.9	H	1.1
$\nu p_{3/2}$	$\nu[521]\frac{1}{2}^-$	M	0.8	–	
$\pi g_{7/2}$	$\pi[404]\frac{7}{2}^+$	a	0	b	0
$\pi d_{5/2}$	$\pi[402]\frac{5}{2}^+$	c	0	d	0
$\pi i_{13/2}$	$\pi[660]\frac{1}{2}^+$	m	5.7	–	
$\pi h_{11/2}$	$\pi[514]\frac{9}{2}^-$	e	1.7	f	1.7
$\pi h_{9/2}$	$\pi[541]\frac{1}{2}^-$	g	3.8	–	

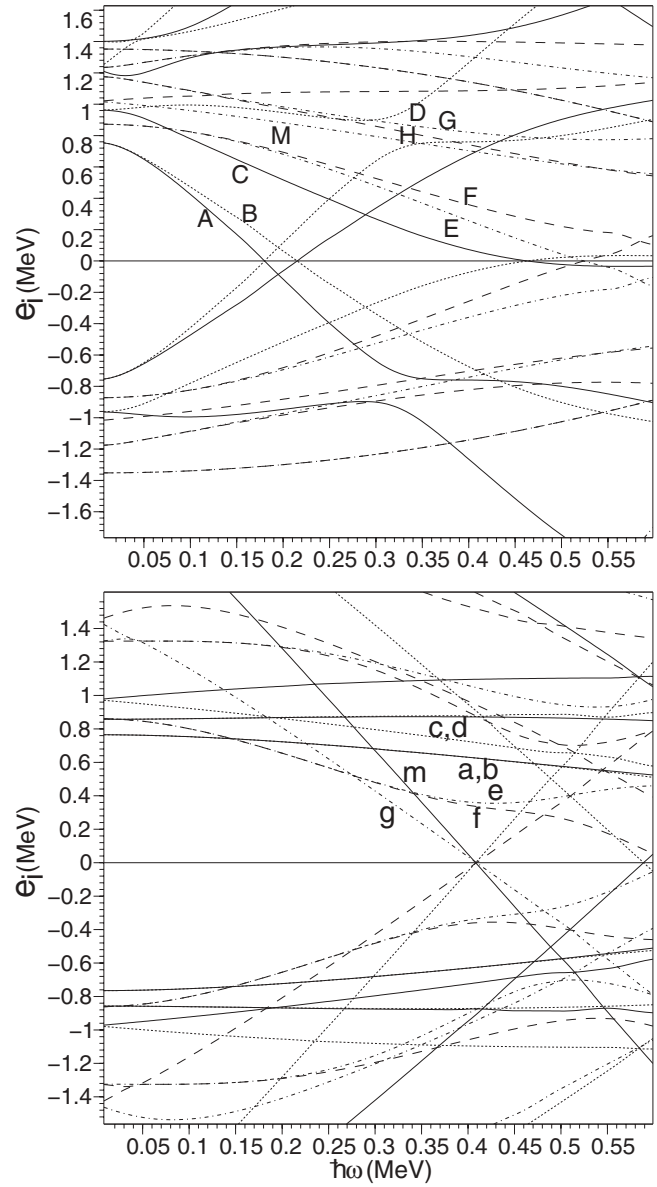

FIG. 5. Quasiparticle diagram for neutrons (upper panel) and protons (lower panel) for ^{168}Hf calculated at $\beta_2 = 0.250$, $\beta_4 = 0.02$, and $\gamma = 0^\circ$. The levels are labeled by parity and signature as $(+,+1)$ solid lines, $(+,-1)$ dotted lines, $(-,+1)$ dot-dashed lines, and $(-,-1)$ dashed lines.

TABLE III. Summary of configurations, observed and UC calculated band crossing frequencies (in keV), and observed alignment gain i_x (in $\hbar$) in ^{168}Hf.

Band	Config.	Crossing	$\hbar\omega_{exp}$	$\hbar\omega_{cal}$	$\Delta\hbar\omega$	i_x
1	G	AB	265	200	+65	9.0
		fg	550	480	+70	6.1
2	GBC	AD	360	320	+40	
3	AE	BC	300	290	+10	7.0
		fg	540	480	+60	5.2
4	AF	BC	290	290	+0	6.8
		fg	550	480	+70	>3.5
5	BE	AD		320		
6	AM	BC	320	290	+30	4.5
7	AG	BC	300	290	+10	5.4
8	AH	BC	300	290	+10	6.2
11	(ga/gb)AB					
12	(ge/gf)BE					
13	(ge/gf)AE	BC	315	290	+25	6.0

A. Bands 1–10

1. Bands 1 and 2

Band 1, the ground band or quasiparticle vacuum, is crossed by the two-quasineutron band AB [see Fig. 6(a)]. This sharp crossing, indicating a very weak interaction between the two bands, occurs systematically at $\hbar\omega \approx 260$ keV in $N = 96$ nuclei, such as ^{166}Yb [23], ^{167}Lu [24], ^{169}Ta [25], and ^{170}W [26]. The alignment gain of $i_x \sim 9\hbar$ is reproduced well by the calculations. In contrast, in $N = 98$ nuclei (e.g., ^{170}Hf [7]), a strong interaction at the AB crossing results in a very gradual alignment pattern. A further gradual increase in alignment is observed in Band 1 of ^{168}Hf between $\hbar\omega \approx 330$ and 480 keV. A similar increase is also observed in the Band AB of ^{166}Hf [17], which was attributed to either the neutron CD alignment or to a mixture of CD and EF alignments with a strong interaction. Such an interpretation is probably also valid for the AB band in ^{168}Hf. The sharp alignment at $\hbar\omega \approx 550$ keV will be discussed in Sec. IV B.

Band 2, the continuation of Band G, is crossed by the BC band at $\hbar\omega \approx 290$ keV; the latter then undergoes the AD crossing at $\hbar\omega \approx 320$ keV. The rather large total alignment of $12.5\hbar$, about $1\hbar$ larger than that in Band 1, suggests that the EF crossing is also involved. Band 2 is observed to interact with the GAB band via eight $E2$ interband transitions between spins 14^+ and 30^+, which indicates some mixing between the bands.

2. Bands 3–6

Bands 3 and 4 were previously identified as associated to AE and AF configurations [16]. Indeed, these two bands have the lowest excitation energies, except for the yrast GAB band, within a wide spin region $I = 10$–36 [see Fig. 7(a)]. The most pronounced feature in the two bands, seen in Fig. 6(a), is the BC crossing at $\hbar\omega \approx 300$ keV, confirming that their intrinsic configuration contains quasiparticle A, and, consequently, the AB crossing is blocked. Band 3, the positive signature AE, gains about $7\hbar$ of aligned angular momentum, while Band 4, the negative signature AF, gains slightly less. The appearance of another crossing at frequency $\hbar\omega \approx 540$ keV will be discussed in Sec. IV B. The initial alignment of Band 3 (AE) is, contrary to expectation, less than that of Band 4 (AF). This is explained below by the interaction between Bands 3 and 6.

Band 5 has a higher excitation energy than the AF configuration for spins greater than $10\hbar$ [see Fig. 7(a)]. Its alignment has a clearly different pattern than those of the AB crossing seen in Band 1 and the BC crossing seen in Band 4 [Fig. 6(a)]. It was identified by Beck *et al.* [16] as the AD crossing around $\hbar\omega \sim 320$ keV, implying that its intrinsic configuration includes quasiparticle B. We concur with this as well as with the BE configuration assignment for Band 5 [16]. The exact amount of alignment gain resulting from the AD crossing is difficult to determine because the alignment curve continuously rises from lower frequencies. The band decays to AE and AF sequences through a number of $M1$ and $E2$ transitions, respectively.

Band 6 is higher than the AE sequence but lower than BE band in excitation energy [Fig. 7(a)]. It cannot be associated with the BF configuration, which should have a higher excitation energy than that of the BE configuration. Band 6 experiences a slightly delayed BC crossing, similar to Bands 7 and 8 (AG and AH, as discussed below), see Fig. 6(b).

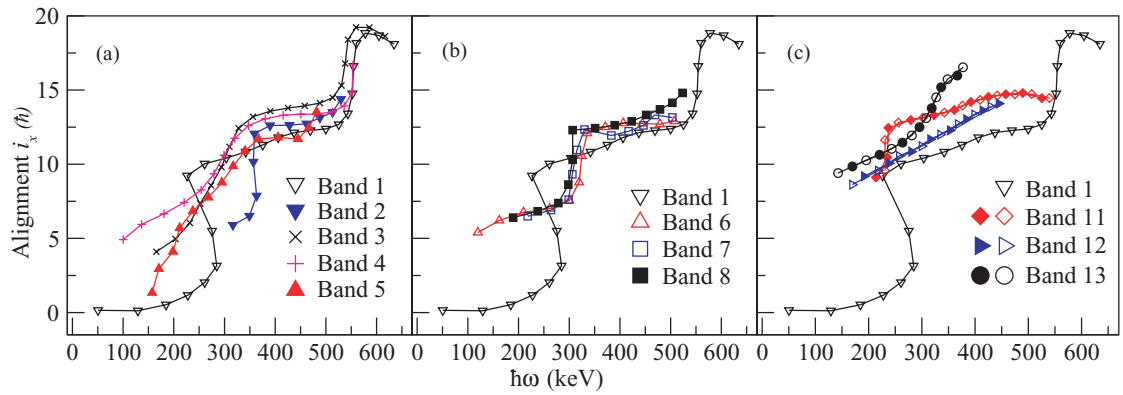

FIG. 6. (Color online) Alignments for the bands in ^{168}Hf. Harris parameters $J_0 = 25\hbar^2$ MeV^{-1} and $J_1 = 53\hbar^4$ MeV^{-3} were used to subtract the angular momentum of the rotating core. Filled (open) symbols denote $\alpha = 0(1)$ sequences for the strongly coupled Bands 11, 12, and 13, which are plotted with $K = 4$, 10, and 10, respectively (see text for details).

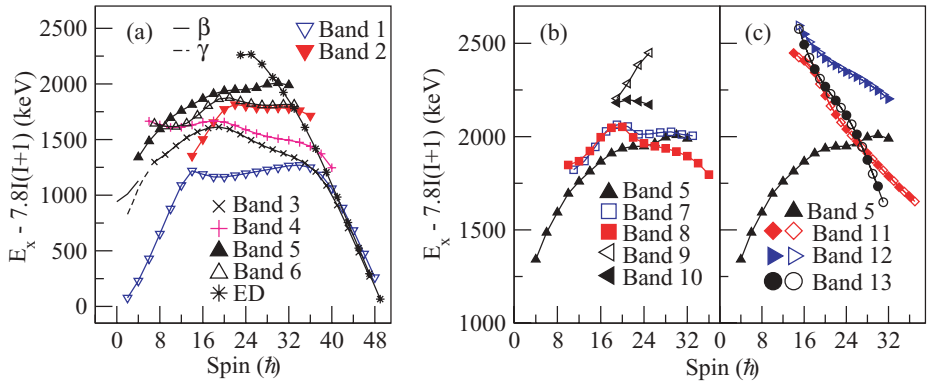

FIG. 7. (Color online) Excitation energies, minus a rigid rotor reference, as a function of rotational frequency for the bands in ^{168}Hf. An inertia parameter $A = 7.8$ was used. Filled (open) symbols denote $\alpha = 0(1)$ sequences for Bands 11−13.

This rules out further the possibility of a BF configuration assignment for Band 6, indicating that quasiparticle A is, instead, involved. For the second neutron orbital in Band 6, the only remaining possibility is the M orbital, because the G and H ones are already identified in Bands 7 and 8. It is worth pointing out that the calculated energies of several neutron orbitals are dependent on deformation, even the EF and MN orbital pairs could be switched. Experimentally, this $[521]1/2^-$ (M) orbital is found in numerous nuclei in this region. It is the ground state of the $N = 101$ isotones ^{169}Er, ^{171}Yb, and ^{173}Hf [21]. It is also found as an excited state of the $N = 99$ isotones ^{167}Er, ^{169}Yb, ^{171}Hf [21], the $N = 98$ isotope ^{170}Hf [7], and the $N = 97$ isotones ^{167}Yb [21] and ^{169}Hf [27]. This orbital is observed to be as low as the $\alpha = -1/2$ signature of the $[523]5/2^-$ orbital in ^{169}Hf and lower than the $[521]3/2^-$ orbital in ^{170}Hf. These facts leave us confident in our configuration assignment of AM to Band 6. The signature partner of Band 6 is not observed because of the expected strong signature splitting.

The low spin regions of Bands 3, 5, and 6 require some further discussion. It is quite obvious in Fig. 7(a) that Band 4 (AF) is a partner with Band 6 at spins $I \lesssim 14$ but with Band 3 at $I \gtrsim 18$. However, Band 3 at low spins and Band 6 at high spins may well have the same intrinsic configuration AM. Further proof of this rather smooth (strong) interaction between Bands 3 and 6 comes from the $E2$ transitions from Band 6 (between 23^- and 11^-) to Band 3. Similarly, $M1$ transitions are found to decay from levels between 20^- and 12^- in Band 4 (AF) to levels in Band 3 (AE). In the lower-spin regions there are $M1$ transitions between Bands 4 and 6. All these facts are consistent with a scenario where Band 6 is associated with the AE configuration at low spins. Thus, there is a character exchange between Bands 3 and 6 around spin 16. It is not clear why the energy levels of low-spin states in the BE configuration (Band 5) are lower than those in AE (low-spin levels in Band 6). Beck *et al.* [16] suggested that the low-spin states of Band 5 could be mixed with an octupole vibrational band, which causes the lowering of the energies of these states, or be interpreted as the continuation of an octupole band [16]. A similar interpretation was suggested for the abnormally low energy levels in the BE band of ^{166}Yb [28]. It is also unclear why the BF configuration, the signature partner of BE, is not observed. A possibility is that if BE is mixed with the unobserved signature partner of AM, or lowered through mixing with it, then the splitting between the BE and BF sequences could be larger than the expected EF splitting.

3. Bands 7–10

Bands 7 and 8 undergo the BC crossing [Fig. 6(b)] at $\hbar\omega \sim 300$ keV with aligned angular momenta of ∼5.4 and 6.2$\hbar$, respectively, indicating that the quasineutron orbital A is contained within their respective intrinsic configurations. The bands have higher excitation energy than those associated with the AM and BE configurations. As can be seen in Fig. 7(b), they are clearly partners. In the region of rotational frequency $\hbar\omega \approx 0.3$–0.5 MeV, the signature splitting is apparent, yet smaller than the splitting seen between the AE and AF configurations. Band 8 ($\alpha = -1/2$) lies lower than Band 7. All these facts are consistent with the UC predicted G and H orbitals for Bands 7 and 8. Therefore, the AG and AH configurations are proposed for Bands 7 and 8, respectively.

Bands 9 and 10 are very short. With this limited knowledge of their experimental properties, it is difficult to gain a solid understanding of their intrinsic configurations. We can only consider some possibilities. Band 9 has positive parity, odd spins, and an excitation energy higher than Band 2 (GBC); it could represent the extension of the Band G with an AC alignment. Band 10 has negative parity, odd spins, and an excitation energy higher than Band 5 (BE). These quantities are consistent with those required for the unobserved BF band.

B. High-spin proton crossing

Bands 1, 3, and 4 exhibit another crossing at higher rotational frequency ($\hbar\omega \sim 540$–550 keV). The full alignment gain of 5.2$\hbar$ in Band 3 and 6.1$\hbar$ in Band 1 can be deduced from Fig. 6(a). The beginning of this crossing can also be noticed in Band 2. This crossing must involve quasiprotons because it is observed as a general phenomenon in bands with different neutron configurations that have been observed to sufficiently high spins. The large alignment gain cannot be explained by excitation of the e and f quasiprotons (based on the $[514]9/2^-$ orbital) alone. The g quasiproton (based on the $[541]1/2^-$ orbital), which has a large alignment and is predicted to cross the e orbital around $\hbar\omega \sim 480$ keV (see Fig. 5), must be involved as well. Note that the calculated crossing frequency is very deformation dependent and that the ∼25 keV difference in crossing frequencies between the bands AEBC (Band 3) and AFBC (Band 4) may indicate a signature dependence on deformation. The $[541]1/2^-$ (g) orbital is close to the proton Fermi surface for $^{168}_{72}$Hf, and yrast bands in both $^{167}_{71}$Lu [24] and $^{169}_{73}$Ta [25] are based on this orbital, which is known to drive

nuclei to larger deformation and to cause a delay in the crossing frequency of the first neutron pair. The mixed fg crossing from the $[514]9/2^-$ and $[541]1/2^-$ orbitals is predicted to generate about $5.5\hbar$ of aligned angular momentum, in agreement with the alignment observed. Therefore, at high spin Band 3 is assigned AEBCfg, while Band 1 is assigned ABCDfg with the understanding that some mixture with ABEFfg is probably present.

Alternatively, one might consider the mb configuration or $\pi[660]1/2^+(\alpha = +1/2) \otimes \pi[404]7/2^+(\alpha = -1/2)$. The UC calculations indicate that the alignment of this pair may occur around frequencies $\hbar\omega \sim 500$ keV. The pronounced down-sloping of the $\pi[660]1/2^+$ orbital as a function of rotational frequency is well known, and this orbital alone is expected to contribute about $5.7\hbar$ to the alignment. This orbital has been identified in neighboring Lu isotopes (^{163,165,167}Lu [2–5]), where it drives nuclei to large, significantly triaxial deformations that produce wobbling families of TSD bands. The orbital has also been observed in neighboring Ta isotopes ^{169,171}Ta [25,29] and very recently in ^{167}Ta [30]. In each of these cases, the $[660]1/2^+$ orbital is located higher than the $[541]1/2^-$ one, allowing the latter to align more easily. In ^{168}Hf, the $\pi[660]1/2^+$ orbital has also been identified in Band ED [15] where the nucleus has an enhanced deformation ($Q_t \approx 9\ e$ b) relative to the ND structures ($Q_t \approx 5.9\ e$ b) [31,32]. Therefore, the configuration mb is believed to be less likely for the above-mentioned proton alignment. Similar conclusions were reached from previous cranked shell-model calculations for ^{166}Hf [17], ^{167}Hf [33], and ^{169}Hf [27,34]. Such a mixed proton alignment has previously been observed in other rare-earth nuclei, such as ^{165,166}Yb [23], ^{167,168}Yb [35], and ^{170}W [26]. Only in recent years, however, have the bands been observed to sufficiently high spins in several nuclei so that the full alignment can be ascertained. Consequently, this proton mixed fg crossing can now be firmly established.

C. Strongly coupled bands and coexisting alignment schemes

The large initial alignment at low spins and the high excitation energy of Bands 11–13 suggest that these bands are associated with a four quasiparticle structure consisting of two quasineutrons and two quasiprotons. In addition to the rotational properties of the bands, such as their alignment patterns, excitation energies, moments of inertia, and the Routhians, the $B(M1)/B(E2)$ ratios are very useful for revealing the intrinsic configurations of strongly coupled bands. Detailed comparisons were also carried out with similar bands in neighboring nuclei.

1. B(M1)/B(E2) ratios

For strongly coupled bands with $\Delta I = 1$ mixed $M1/E2$ connecting transitions, the experimental values of $B(M1, I \rightarrow I-1)/B(E2, I \rightarrow I-2)$ ratios have been extracted from the expression

$$\frac{B(M1)}{B(E2)} = 0.693 \frac{T_1}{T_2} \frac{E_2^5}{E_1^3} \frac{1}{1+\delta^2}, \qquad (1)$$

where subscripts 1 and 2 refer to the $\Delta I = 1$ and $\Delta I = 2$ transitions, respectively. The quantities T and E are the γ-ray intensity and energy (in MeV). The mixing ratio $\delta^2 = T_1(E2)/T_1(M1)$ was neglected in the calculations. The effect from the mixing ratio on the calculated $B(M1/B(E2)$ values of strongly coupled bands in ^{166}Hf [17] was estimated to introduce a $\lesssim$10% correction, based on the results of rigid-rotor calculations. Thus, the "experimental values" should be understood as upper limits of the actual $B(M1, I \rightarrow I-1)/B(E2, I \rightarrow I-2)$ ratios. The calculated $B(M1)$ values are based on an extension of the geometrical model of Ref. [36]

$$B(M1, I \rightarrow I-1) = \frac{3}{8\pi I^2} \left\{ \sqrt{I^2 - K^2} \left[\sum_J (g_J - g_R)\Omega_J \right] - K \left[\sum_J (g_J - g_R)\iota_J \right] \right\}^2 \mu_N^2. \qquad (2)$$

The theoretical value for the collective gyromagnetic ratio was calculated to be $g_R = 0.35$ in Ref. [37]. A smaller value of $g_R = 0.31$ was used in our calculations to take into account the change in the moment of inertia at high spins due to the decrease in neutron pair correlations. The intrinsic g factors, g_J, used for different quasiparticle orbitals (see Table II) are taken from Ref. [17], where they have been calculated from the wave functions in Ref. [38] to be A, B, C, D: -0.28; E, F: 0.25; G, H: -0.61; e, f: 1.29; g: 0.76; a, b: 0.63. A value of 1.57 was taken for orbitals c and d from Ref. [25]. For the aligned quasineutron pairs AB and BC summed alignments of 9 and $6\hbar$ have been used, respectively, together with a zero contribution to K values. The standard rotational form of the $B(E2)$ strength was calculated using the expression [1]

$$B(E2, I_i \rightarrow I_f) = \frac{5}{16\pi} Q_t^2 \langle I_i K 20 | I_f K \rangle^2 \qquad (3)$$

with $Q_t = 5.9\ e$ b [31,32] adopted for the transition quadrupole moment.

2. Bands 11 and 12

The aligned angular momentum of Band 11 is plotted in Fig. 6(c) assuming $K = 4$. A crossing is observed at the rotational frequency $\hbar\omega \sim 240$ keV, where the AB crossing occurs in Band 1 (GAB). Band 11 has an alignment $\sim 3\hbar$ higher than that of the GAB band. Otherwise, the alignment pattern of the two bands is basically identical, including the gradual rise of the alignment curve caused by the CD crossing or an admixture of CD and EF crossings with strong interaction. Such crossings can also be seen from the dynamic moment of inertia of Band 11 (Fig. 8), which exhibits an increase in a broad region of rotational frequency $\hbar\omega \gtrsim 330$ (spin > 20). Band 11 is, therefore, associated with the AB neutron configuration. To account for the additional $\sim 3\hbar$ in aligned angular momentum, possible proton configurations, constructed from low-lying proton orbitals close to the Fermi surface, may be ga/gb, ge/gf, or fa/fb. The fa/fb pair is predicted to generate less than $2\hbar$ in aligned angular momentum. Calculated $B(M1)/B(E2)$ ratios for the (faAB,fbAB) configuration are far from the experimental values [see Fig. 9(a)]. However, the ge/gf pair is predicted to generate an overly large ($\sim 5.5\hbar$)

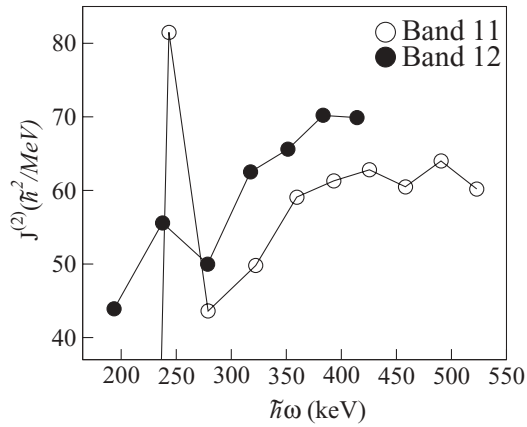

FIG. 8. Dynamic moments of inertia $J^{(2)}$ as a function of rotational frequency for the strongly coupled Bands 11 and 12. Only one signature is shown for each band.

aligned angular momentum. It also has a positive parity, in contrast with our assignment. The $B(M1)/B(E2)$ ratios computed for a (geAB,gfAB) configuration, especially in lower-spin region, are also much larger than the experimental values. At spin $I > 20$, the experimental $B(M1)/B(E2)$ ratios increase slightly, possibly caused by additional crossings. The expected alignment of the ga/gb pair is $3.8\hbar$, close to the observed value. The calculated $B(M1)/B(E2)$ ratios for the (gaAB,gbAB) configuration are closer to the experimental values than is the case for the former two configurations. Furthermore, it was observed in the neighboring ^{169}Ta nucleus that there is a strong mixing between the bands built on $\pi g_{7/2}[404]7/2$ (a and b) and $\pi d_{5/2}[402]5/2$ (c and d) orbitals, which results in rather close $B(M1)/B(E2)$ ratios for the two bands [25]. The same may occur here for Band 11. The (gcAB,gdAB) and (gaAB,gbAB) configurations are expected to generate similar aligned angular momentum. The calculated $B(M1)/B(E2)$ ratios for the (gcAB,gdAB) configuration are slightly higher than the ratios for the (gaAB,gbAB) one and are thus closer to the experimental values. Based on these considerations, Band 11 is proposed to be associated with a mixture of the (gaAB,gbAB) and (gcAB,gdAB) configurations with $K \approx 3.5$. The band decays to the GAB band ($K^\pi = 0^+$) before reaching its band head. The effect of the uncertainty of the quadrupole moment Q_t on the calculated $B(M1)/B(E2)$ ratios is displayed in Fig. 9(a). The ratio increases slightly when Q_t is reduced by 10%.

Band 12 starts from a rotational frequency below the neutron AB crossing frequency (the exact frequency depends on the K value assumed); see Fig. 6(b). The band exhibits neither an AB nor BC crossing. This suggests that it probably contains the quasineutron orbital B. The other quasineutrons could be E, F, G, or H. The lowest combination of one of these with B is BE, which should be common for the two signatures of Band 12. If one signature contains BE and the other contains BF, the band would exhibit a splitting corresponding to the splitting between orbitals E and F. Band 12 continuously gains angular momentum with increasing rotational frequency. Dynamic moments of inertia for Band 12 (Fig. 8) indicate that, similar to Bands 11 and 1, there is a band crossing with a

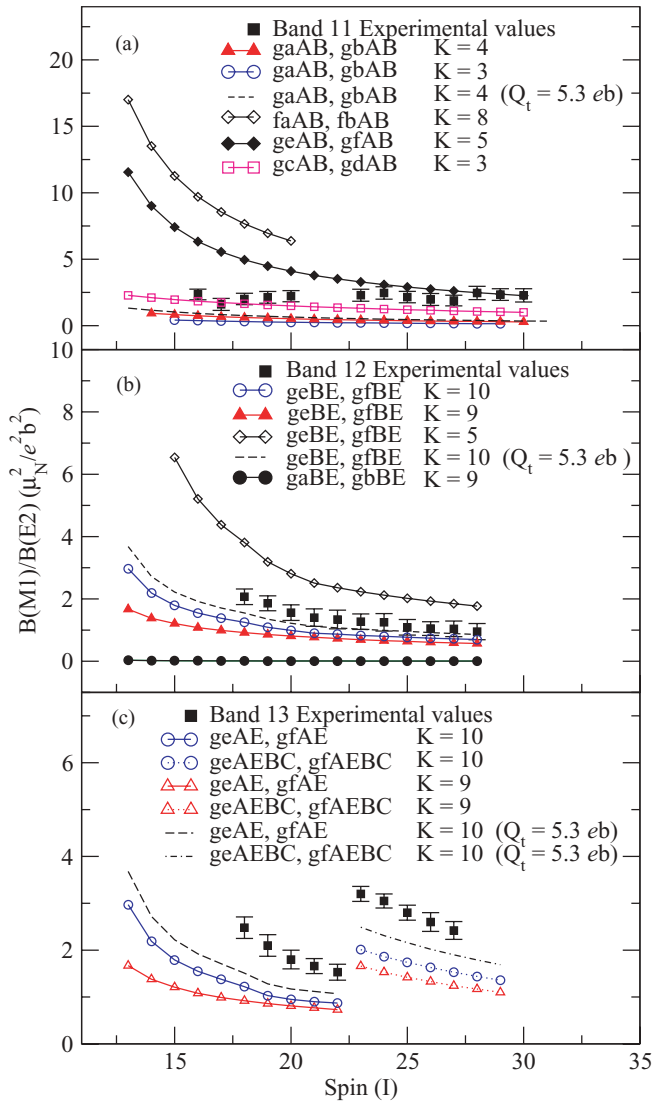

FIG. 9. (Color online) Experimental $B(M1)/B(E2)$ ratios of Bands 11−13 compared to theoretical values for relevant configurations. See text for a detailed discussion.

strong interaction in a broad region between the frequencies $\hbar\omega \approx 330$ and 480 keV, presumably caused by the CD crossing or an admixture of CD and EF crossings. Below this region, the gain of angular momentum most likely comes from a gradual increase in alignment of the intrinsic quasiparticles, which may not be fully aligned at the lowest spins. Band 12 has $8.7\hbar$ initial alignment and continuously gains angular momentum up to $\sim 12\hbar$ when all intrinsic quasiparticles are fully aligned. Excluding $\sim 6.3\hbar$ from the BE combination, the two quasiprotons generate $5.5\hbar$ alignment. The proton configuration ge/gf seems to be the most probable candidate. Another combination ga/gb could only produce $\sim 3.8\hbar$ alignment (and result in a positive-parity band). The $B(M1)/B(E2)$ ratios of several possible configurations are compared in Fig. 9(b). The calculated values for the (geBE, gfBE) configuration coupled to $K = 10$ seem to be in the best agreement with the experimental values. Therefore, the full configuration for

band 12 is suggested to be $\pi([541]1/2^-, [514]9/2^-)_{K=5} \otimes \nu([642]5/2^+, [523]5/2^-)_{K=5}$, coupling to $K^\pi = 10^-$.

Band 12 decays out at $I = 15$ before reaching the bandhead. It decays mainly to the GAB band with $\triangle K = 10$, which makes the transition K forbidden. One of the possible reasons for such a decay is that the constituent orbitals of the band $\pi[541]1/2^-$ and $\nu[642]5/2^+$ both have large alignments. These orbitals may introduce a distribution in K around the $K = 10$ value. Second, the yrast GAB band may not have a pure $K = 0$ structure around spin 14 because the Coriolis force can mix high-K components into its wave function. Such mixing arguments have been employed to explain, for example, the anomalous $\triangle K = 14$ decay of an isomeric state to the $K = 0$ yrast states in ^{174}Hf [39], the $\triangle K = 12$ decay of an isomeric state in ^{172}Hf [40], as well as the short lifetime of a $K = 6$ isomeric state in ^{172}Hf [41]. In addition, TSD bands have been identified in ^{168}Hf [15] and, hence, triaxiality may play a role here. For a triaxial nucleus, K is not a good quantum number and thus K mixing becomes possible. This decay mechanism involves the nuclear shape tunneling through the potential barrier in the γ degree of freedom. It has been used to explain, for example, the decays of a $K = 25$ isomer in ^{182}Os [42] and a $K = 14$ isomer in ^{176}W [43].

3. *Band 13: coexisting rotation and deformation alignments*

Band 13 starts from a rotational frequency of $\hbar\omega \sim 140$ keV and then undergoes the BC crossing at $\hbar\omega \sim 310$ keV (depending on the K value used) with a gain of $6\hbar$ in aligned angular momentum [see Fig. 6(c)]. The band must contain quasineutron orbital A. The other quasineutrons could therefore be E, F, G, or H. The lowest combination of one of these with A is AE. The initial alignment of the band is $1\hbar$ larger than that of Band 12. Based on the considerations for proton orbitals used for band 12, the ge/gf configuration seems again to be the most probable candidate for Band 13, which creates a full configuration (geAE, gfAE) for Band 13. The $1\hbar$ higher alignment compared to Band 12 comes from the difference between the neutron AE orbitals in Band 13 and BE in 12. At the lowest spins, Bands 12 and 13 have similar excitation energies [see Fig. 7(c)], because the only difference in the two sequences is the A and B orbitals, which are close in energy. The initial excitation energy of Band 11 is substantially lower due to its neutron AB configuration, which is much lower than BE (AE) in Band 12 (13). $B(M1)/B(E2)$ ratios were calculated as a function of spin for several configurations. In addition to the proton configurations mentioned for Band 12, the ma/mb combination, or $\pi([660]1/2^+, [404]7/2^+)$, was also considered. Its theoretical $B(M1)/B(E2)$ ratios are, however, too low compared to the experimental values. The calculated ratios for the (geAE,gfAE) configuration with $K = 10^-$ have the best agreement with the experimental values, which are presented in Fig. 9(c). The agreement is fairly good below and above $I = 23^-$ where the BC crossing occurs. Accordingly, the configuration for Band 13 is proposed to be $\pi([541]1/2^-, [514]9/2^-) \otimes \nu([642]5/2^+, [523]5/2^-)$ coupling to $K^\pi = 10^-$. Similar to Band 12, Band 13 decays at $I = 15$ to the GAB band. This transition with a $\triangle K = 10$ hindrance could also be explained by the K mixing and the γ softness as discussed above for Band 12.

Bands 13 and 3 both possess a six-quasiparticle nature at their highest spins, where they appear to have identical quasiparticles, namely gfAE(BC) and geAE(BC) for the two signatures of Band 13 and AE(BC)(gf) for Band 3. The use of quasiparticle labels, though, cannot be justified for both bands that are obviously quite different. In the AEBC band the two quasiprotons align their angular momenta along the rotational axis at high spin, as expected from the UC calculations in which principal axis cranking (PAC) is realized. In the coupled (high-K) band, the quasiprotons must be coupled primarily to the deformation axis. The high-K band is not a solution expected from PAC calculations. The high spin parts of the two bands, therefore, realize different couplings of particles in identical orbitals. These couplings result in a difference in aligned angular momentum of $\sim 2.5\hbar$ [see Fig. 6(c)].

The observation of coexisting rotation and deformation alignments of six-quasiparticle bands based on identical quasiparticle orbitals in ^{168}Hf is the second example observed for such a rather exotic phenomenon. Previously, it had only been observed in ^{166}Hf [17], where bands built on these same orbitals, AE(BC)(gf) for the rotational aligned band and geAE(BC)/gfAE(BC) for the high-K band were observed. The rotation aligned band was found to lie a few hundred keV lower than the coupled band. It was suggested that the difference can be traced to different couplings of the two protons with four spectator neutrons and that such a coexistence is probably analogous to the cases of s- and t-bands representing aligned and tilted coupling of the $i_{13/2}$ quasineutrons in neutron-rich rare-earth nuclei [44]. Such rather exotic cases of six-quasiparticle bands call for more advanced theoretical calculations.

V. SUMMARY

High-spin normal deformed structures in ^{168}Hf have been investigated thoroughly. The six previously known bands have been extended to significantly higher spins. Seven new bands have been established of which three are strongly coupled in nature. Spins and parities have been assigned firmly based on DCO ratio measurements backed by a study of the intrinsic configurations of the bands. All new bands, except Band 9, have been assigned negative parity. Intrinsic configurations of the bands have been investigated based on cranking calculations performed with the ULTIMATE CRANKER code and on systematic comparisons with neighboring nuclei.

At low spins, the bands have been assigned two- or four-quasiparticle configurations. Bands 1 (GAB) and 3 (AE) have been extended to spins as high as 48^+ and 47^-, respectively, so that the band crossings at a frequency $\hbar\omega \sim 0.55$ MeV can be fully delineated. These crossings are proposed to be built on proton excitations in a mixed crossing involving the proton orbitals $h_{11/2}, \alpha = -1/2(f)$ and $h_{9/2}, \alpha = +1/2(g)$. The onset of the proton crossing, resulting in six-quasiparticle structures, is observed in several other bands as well.

One strongly coupled high-K band, Band 13, has been assigned the six-quasiparticle configuration involving the $\pi[541]1/2^-, \pi[514]9/2^-, \nu[642]5/2^+, \nu[651]3/2^+$, and

$\nu[523]5/2^-$ orbitals, identical to those involved in Band 3 (AE) at the highest spins. While Band 3 represents a case of rotational alignment, Band 13 is built on deformation alignment. These two couplings result in a difference in aligned angular momentum. Such a coexistence of coupling schemes based on identical quasiparticle orbitals has previously only been observed in ^{166}Hf [17].

ACKNOWLEDGMENTS

This work was supported by the US Department of Energy, Office of Nuclear Physics, under Grants DE-FG02-95ER40939 (MSU) and DE-AC02-06CH11357 (ANL), the Danish Natural Science Foundation, the German BMBF under Grant 06BN109, and the Research Council of Norway.

APPENDIX

TABLE AI. γ-ray energies, intensities, DCO ratios, and suggested multipolarities in ^{168}Hf.

I_i^π[a]	E_i (keV)[a]	E_γ (keV)[a]	I_γ[b]	R_{DCO}	Assignment
		Band 1			
0^+	0.0				
2^+	123.9	123.6	23(2)		$E2$
4^+	385.6	261.3	100(3)	1.09(10)	$E2$
6^+	756.8	371.0	100(3)	1.40(15)[c]	$E2$
8^+	1213.3	456.3	96(3)	1.42(16)[c]	$E2$
10^+	1735.6	522.4	81(3)		$E2$
12^+	2305.7	570.0	70(3)	1.09(11)	$E2$
14^+	2857.0	551.3	45(2)	0.98(10)	$E2$
16^+	3309.9	452.9	45(3)		$E2$
		319.8	2.0(2)		$E2$
18^+	3832.0	521.9	43(3)		$E2$
20^+	4439.5	607.3	19(2)	0.95(9)	$E2$
22^+	5123.8	684.1	24(3)		$E2$
24^+	5875.0	751.0	15(1)		$E2$
26^+	6687.5	812.2	13(2)		$E2$
28^+	7562.6	874.8	8.0(9)		$E2$
30^+	8501.4	938.8	4.1(5)		$E2$
32^+	9501.1	999.7	2.7(4)		$E2$
34^+	10551.8	1050.7	1.6(3)		$E2$
36^+	11638.6	1086.8	1.0(2)		$E2$
38^+	12743.3	1104.7	0.7(1)		$E2$
40^+	13852.1	1108.8	0.7(1)		$E2$
42^+	14972.6	1120.5	0.8(1)		$E2$
44^+	16128.1	1155.5	1.0(2)		$E2$
46^+	17337.2	1209.1	0.8(1)		$E2$
48^+	18606	1269	0.7(1)		$E2$
		Band 2			
14^+	2990.1	684.5	13.5(6)		$E2$
16^+	3623.6	766.6	3.6(4)		$E2$
		633.5	15(2)		$E2$
18^+	4321.9	1012.0	<0.5		$E2$
		698.3	4.4(7)		$E2$
20^+	5048.8	726.9	5.3(6)		$E2$
22^+	5762.9	1323.4	1.0(2)		$E2$
		714.1	2.3(3)		$E2$

TABLE AI. (*Continued*.)

I_i^π[a]	E_i (keV)[a]	E_γ (keV)[a]	I_γ[b]	R_{DCO}	Assignment
24^+	6481.0	1357.3	1.1(1)	1.02(17)	$E2$
		718.3	3.2(4)		
26^+	7260.5	1385.5	0.7(1)	0.94(12)	$E2$
		779.8	1.4(2)		$E2$
28^+	8116.8	1429.3	<0.5		$E2$
		856.4	1.5(2)		$E2$
30^+	9040.5	1477.6	<0.5		$E2$
		923.9	1.5(2)		$E2$
32^+	10016.7	976.2	1.1(1)		$E2$
34^+	11042.9	1026.2	0.6(1)		$E2$
36^+	12102	1059	0.5(1)		$E2$
		Band 3			
7^-	1734.9	978.0	5.0(5)		$E1$
9^-	2066.6	853.0	6.2(7)	0.80(8)	$E1$
		331.8	0.7(1)	0.97(12)	$E2$
11^-	2473.6	738.0	8.4(8)	0.64(14)	$E1$
		406.9	3.6(4)	0.97(14)	$E2$
13^-	2937.3	631.7	9.8(9)	0.62(9)	$E1$
		463.7	13.5(9)	0.98(10)	$E2$
15^-	3441.7	504.4	16(2)	0.97(10)	$E2$
		451.6	1.6(2)		$E1$
17^-	3989.1	547.4	14(2)	1.03(10)	$E2$
		365.5	<0.5	0.55(8)	$E1$
19^-	4577.3	588.2	12(2)	0.99(5)	$E2$
		255.4	<0.5		$E1$
21^-	5196.8	619.5	10(2)	1.02(10)	$E2$
23^-	5852.8	656.0	8.8(5)	1.02(9)	$E2$
25^-	6565.1	712.3	6.9(9)	1.03(9)	$E2$
27^-	7346.2	781.1	5.3(7)	1.02(9)	$E2$
29^-	8196.9	850.7	5.6(8)	0.93(8)	$E2$
31^-	9113.6	916.7	2.6(4)	0.99(9)	$E2$
33^-	10090.1	976.5	1.7(3)	0.99(9)	$E2$
35^-	11117.1	1027.0	1.4(2)	1.06(7)	$E2$
37^-	12178.6	1061.5	1.1(2)	1.09(10)	$E2$
39^-	13254.8	1076.2	0.5(1)	0.96(12)	$E2$
41^-	14342.0	1087.2	0.5(1)		$E2$
43^-	15461.1	1119.1	<0.5	1.04(12)	$E2$
45^-	16632.3	1171.2	<0.5	1.03(9)	$E2$
47^-	17866	1234	<0.5		$E2$
		Band 4			
6^-	1992.3	1235.4	1.2(2)	0.85(11)	$E1$
8^-	2193.2	980.0	3.3(4)	0.84(10)	$E1$
		380.0	3.0(6)	0.91(12)	$E2$
		200.9	0.9(1)		$E2$
10^-	2466.4	399.7	0.5(1)		$M1/E2$
		311.2	2.0(2)	0.87(7)	$E2$
		273.2	5.9(6)	0.91(8)	$E2$
		145.4	0.7(1)	0.41(7)	$M1$
12^-	2828.0	361.6	9.2(8)	0.93(9)	$E2$
		182.2	<0.5	0.59(8)	$M1$
14^-	3269.0	441.0	9.2(9)	0.98(8)	$E2$
16^-	3777.2	508.2	8.1(8)	0.98(7)	$E2$
18^-	4335.8	558.6	7.5(9)	1.08(7)	$E2$
20^-	4933.8	598.0	6.3(8)	1.05(8)	$E2$
22^-	5574.1	640.3	4.4(6)	1.02(9)	$E2$
24^-	6268.6	694.4	3.3(4)	1.03(9)	$E2$

TABLE AI. (*Continued*.)

I_i^π [a]	E_i (keV)[a]	E_γ (keV)[a]	I_γ [b]	R_{DCO}	Assignment
26^-	7029.3	760.7	2.5(4)	1.02(9)	$E2$
28^-	7860.7	831.4	1.7(2)	1.02(10)	$E2$
30^-	8762.3	901.6	1.0(2)	1.03(8)	$E2$
32^-	9730.7	968.4	0.7(1)	1.02(10)	$E2$
34^-	10756.3	1025.5	<0.5	1.14(14)	$E2$
36^-	11828.5	1072.2	<0.5	0.96(12)	$E2$
38^-	12931.6	1103.1	<0.5	1.02(10)	$E2$
40^-	14038	1107	<0.5	0.99(12)	$E2$
			Band 5		
4^-	1497.2	1111.6	1.5(2)	0.88(12)	$E1$
6^-	1813.2	1056.3	2.2(3)	0.89(15)	$E1$
		316.0	0.5(2)		$E2$
		262.8	1.2(3)		$E1$
		427.4	1.0(1)		$E1$
8^-	2155.2	942.0	1.0(1)	1.06(11)	$E1$
		420.3	1.5(2)		$M1$
		342.0	2.0(5)		$E2$
10^-	2552.6	485.9	0.6(2)	0.72(9)	$M1$
		397.4	2.5(3)	1.05(9)	$E2$
		359.4	1.0(1)		$E2$
		817.0	<0.5		$E1$
12^-	2976.1	509.7	<0.5		$E2$
		502.5	0.9(3)	0.73(10)	$M1$
		423.5	1.9(3)	0.98(11)	$E2$
14^-	3451.6	623.6	<0.5		$E2$
		514.3	<0.5		$M1$
		475.5	2.5(3)	1.06(9)	$E2$
16^-	3988.3	719.3	<0.5		$E2$
		546.6	<0.5		$M1$
		536.7	2.3(3)	1.05(8)	$E2$
18^-	4578.0	800.8	<0.5		$E2$
		589.7	1.8(2)	1.04(10)	$E2$
		588.9	<0.5		$M1$
20^-	5212.8	877.0	<0.5	1.06(8)	$E2$
		635.5	<0.5		$M1$
		634.8	1.5(2)	0.99(11)	$E2$
22^-	5893.6	959.8	<0.5		$E2$
		680.8	1.0(1)	1.03(10)	$E2$
24^-	6628.1	734.5	0.7(1)	1.03(10)	$E2$
26^-	7439.6	811.5	<0.5	1.02(10)	$E2$
		795.2	<0.5	1.09(12)	$E2$
28^-	8329.7	890.1	<0.5	0.94(9)	$E2$
30^-	9262.7	933.0	<0.5	0.99(11)	$E2$
32^-	10226	964	<0.5		$E2$
			Band 6		
7^-	2080.9	1324.0	0.9(2)	0.72(9)	$E1$
9^-	2321.0	1107.8	1.7(3)	0.65(8)	$E1$
		586.1	1.1(2)		$E2$
		240.0	1.0(2)		$E2$
		127.8	<0.5		$M1$
11^-	2645.8	579.1	1.0(2)		$E2$
		324.8	1.5(2)	1.02(12)	$E2$
		179.4	<0.5		$M1$
13^-	3065.6	592.0	0.9(1)		$E2$
		419.8	0.8(2)	0.93(11)	$E2$
		237.6	<0.5		$M1$

TABLE AI. (*Continued*.)

I_i^π [a]	E_i (keV)[a]	E_γ (keV)[a]	I_γ [b]	R_{DCO}	Assignment
15^-	3589.0	651.7	<0.5		$E2$
		523.4	1.0(1)		$E2$
17^-	4189.7	748.0	<0.5		$E2$
		600.7	0.9(1)	0.93(12)	$E2$
19^-	4829.0	639.3	<0.5	1.09(11)	$E2$
21^-	5478.5	1039.0	<0.5		$E1$
		901.2	<0.5	1.04(13)	$E2$
		649.5	0.6(1)	1.10(12)	$E2$
23^-	6150.2	1026.3	<0.5		$E1$
		953.4	<0.5	0.91(9)	$E2$
		671.7	0.5(1)	0.93(10)	$E2$
25^-	6892.5	1017.6	<0.5	1.06(10)	$E1$
		742.3	<0.5	1.06(8)	$E2$
27^-	7705.8	1018.3	<0.5	0.89(10)	$E1$
		813.3	0.5(1)	0.90(13)	$E2$
29^-	8594.3	888.5	<0.5		$E2$
31^-	9552.4	958.1	<0.5	0.91(11)	$E2$
33^-	10567	1015	<0.5	0.94(11)	$E2$
			Band 7		
11^-	2852.0	1116.4	0.7(2)	0.75(10)	$E1$
13^-	3288.6	982.9	<0.5	0.74(10)	$E1$
		436.6	0.8(2)	0.92(14)	$E2$
15^-	3817.1	827.0	<0.5		$E1$
		528.5	1.5(2)	1.19(13)	$E2$
17^-	4414.9	597.8	1.3(2)	0.93(12)	$E2$
19^-	5027.2	612.3	1.3(3)	0.89(14)	$E2$
21^-	5657.7	630.5	0.9(2)	0.98(13)	$E2$
23^-	6318.0	660.3	1.3(3)	1.03(10)	$E2$
25^-	7084.2	766.2	1.3(2)	1.05(13)	$E2$
27^-	7918.7	834.5	<0.5		$E2$
29^-	8811.6	892.9	0.5(1)	1.15(15)	$E2$
31^-	9749.2	937.6	<0.5		$E2$
33^-	10756	1007	<0.5	1.11(16)	$E2$
			Band 8		
10^-	2706.0	970.4	<0.5	0.87(13)	$E1$
12^-	3085.0	379.0	0.9(2)	0.97(15)	$E2$
		233.0	<0.5	0.61(8)	$M1$
14^-	3560.9	475.9	0.9(1)	0.98(11)	$E2$
16^-	4118.5	557.5	0.8(1)	1.03(9)	$E2$
18^-	4715.0	596.5	1.0(2)	0.91(8)	$E2$
20^-	5328.6	613.6	1.3(2)	1.04(13)	$E2$
22^-	5942.2	613.6	1.3(2)		$E2$
24^-	6644.4	702.2	1.1(2)	1.05(10)	$E2$
26^-	7423.6	795.5	0.6(1)		$E2$
		779.2	0.6(1)	0.94(13)	$E2$
28^-	8270.3	846.7	<0.5	1.02(16)	$E2$
30^-	9173.9	903.6	<0.5	0.89(13)	$E2$
32^-	10132.2	958.3	<0.5	0.90(8)	$M1/E2$
34^-	11139.4	1007.2	<0.5	0.89(11)	$M1/E2$
36^-	12186	1047	<0.5		$E2$
			Band 9		
19^+	5168.4	1336.5	<0.5		$M1/E2$
		846.5	1.4(2)	0.91(13)	$M1/E2$
21^+	5888.9	840.1	1.5(2)	0.93(13)	$M1/E2$
		720.5	1.2(2)	1.10(12)	$E2$

TABLE AI. (*Continued*.)

I_i^π [a]	E_i (keV)[a]	E_γ (keV)[a]	I_γ [b]	R_{DCO}	Assignment
23^+	6689.8	926.9	1.4(2)	0.83(18)	$M1/E2$
		800.9	1.1(2)	1.15(12)	$E2$
25^+	7519.7	829.9	1.1(2)		$E2$
(27^+)	8366	846	0.9(1)		$(E2)$
			Band 10		
(19^-)	5146.1	824.2	<0.5		$(E1)$
(21^-)	5801.6	752.8	<0.5		$(E1)$
		655.5	<0.5		$E2$
23^-	6495.0	1371.1	<0.5	0.49(9)	$E1$
		693.4	<0.5		$E2$
25^-	7241.2	1366.3	<0.5	0.69(10)	$E1$
		746.2	<0.5		$E2$
27^-	8037.7	1350.2	<0.5		$E1$
		796.5	<0.5		$E2$
		702.1	<0.5		$E2$
			Band 11		
15^-	4296.4	1439.4	<0.5		$E1$
		1306.3	<0.5	0.90(10)[c]	$E1$
		854.7	<0.5		$M1$
		210.4	0.7(2)	0.96(11)[c]	$M1$
16^-	4528.3	442.3	<0.5	1.39(16)[c]	$E2$
		231.9	1.0(2)	0.78(10)	$M1$
17^-	4772.8	476.4	<0.5	1.49(15)[c]	$E2$
		244.5	0.7(1)	0.76(10)	$M1$
18^-	5011.5	483.2	<0.5	1.61(18)[c]	$E2$
		238.7	<0.5	0.93(10)[c]	$M1$
19^-	5245.8	473.0	<0.5	1.27(15)[c]	$E2$
		234.3	<0.5	0.65(9)	$M1$
20^-	5496.0	484.5	<0.5		$E2$
		250.2	1.9(3)	0.74(8)	$M1$
21^-	5767.9	522.1	<0.5	1.45(16)[c]	$E2$
		271.9	1.8(3)	0.70(8)	$M1$
22^-	6064.6	568.6	<0.5		$E2$
		296.7	2.1(2)	0.75(10)	$M1$
23^-	6381.9	613.9	1.0(2)	0.98(14)	$E2$
		317.2	1.5(2)	0.63(8)	$M1$
24^-	6720.0	655.4	0.7(1)	1.37(15)[c]	$E2$
		338.2	1.1(3)	0.71(8)	$M1$
25^-	7076.1	694.3	0.5(1)	1.05(11)	$E2$
		356.1	0.6(1)	0.95(8)[c]	$M1$
26^-	7451.5	731.5	1.2(2)	1.39(16)[c]	$E2$
		375.4	<0.5	0.97(9)[c]	$M1$
27^-	7838.1	762.0	1.2(2)	1.10(11)	$E2$
		386.6	1.7(2)	0.97(10)[c]	$M1$
28^-	8244.3	792.8	1.3(2)	1.78(25)[c]	$E2$
		406.2	1.3(2)		$M1$
29^-	8665.3	827.2	1.2(3)		$E2$
		421.0	1.6(3)		$M1$
30^-	9102.0	857.7	0.8(1)		$E2$
		436.7	0.6(1)		$M1$
31^-	9556.2	890.9	1.4(2)	0.90(11)	$E2$
		454.2	1.0(2)		$M1$
32^-	10025.0	923.0	1.3(2)		$E2$
		468.8	1.3(2)		$M1$

TABLE AI. (*Continued*.)

I_i^π [a]	E_i (keV)[a]	E_γ (keV)[a]	I_γ [b]	R_{DCO}	Assignment
33^-	10513.2	957.0	0.9(1)		$E2$
		488.2	1.3(2)		$M1$
34^-	11011.3	986.3	1.4(2)		E2
		498.1	0.7(1)		$M1$
35^-	11532.7	1019.5	1.0(2)		$E2$
		521.4	0.7(1)		$M1$
36^-	12069	1058	0.6(1)		$E2$
		536	0.7(1)		$M1$
37^-	12619	1086	<0.5		$E2$
			Band 12		
15^-	4467.3	1610.2	1.0(2)	0.93(15)[c]	$E1$
		843.6	<0.5	1.08(12)[c]	$E1$
16^-	4671.1	203.9	<0.5	0.82(10)	$M1$
17^-	4894.1	426.8	<0.5		$E2$
		223.1	0.8(1)	0.70(8)	$M1$
18^-	5139.1	468.0	<0.5		$E2$
		244.9	0.7(1)	0.78(10)	$M1$
19^-	5412.2	518.0	<0.5		$E2$
		273.1	<0.5	1.03(12)[c]	$M1$
20^-	5695.1	556.0	0.7(1)		$E2$
		282.9	<0.5	1.17(13)[c]	$M1$
21^-	6002.2	590.0	1.0(1)		$E2$
		307.1	0.8(1)	0.63(7)	$M1$
22^-	6329.1	634.0	1.2(2)	0.96(8)	$E2$
		326.9	0.7(1)	0.61(8)	$M1$
23^-	6672.2	670.0	0.7(1)	1.02(15)	$E2$
		343.1	0.6(1)	0.77(9)	$M1$
24^-	7028.1	699.0	<0.5	1.08(11)	$E2$
		355.9	<0.5	0.94(11)[c]	$M1$
25^-	7406.2	734.0	0.5(1)	1.33(22)[c]	$E2$
		378.1	<0.5	1.02(11)[c]	$M1$
26^-	7796.1	768.0	<0.5	1.11(16)	$E2$
		389.9	<0.5	0.72(9)	$M1$
27^-	8201.2	795.0	<0.5	0.92(11)	$E2$
		405.1	<0.5		$M1$
28^-	8620.1	824.0	0.6(1)	1.33(20)[c]	$E2$
		418.9	<0.5		$M1$
29^-	9053.2	852.0	<0.5		$E2$
		433.1	<0.5		$M1$
30^-	9501.1	881.0	<0.5		$E2$
		447.9	<0.5		$M1$
31^-	9963	909	<0.5		$E2$
32^-	10439	938	<0.5		$E2$
			Band 13		
15^-	4449.9	1592.9	<0.5		$E1$
		1459.8	<0.5		$E1$
		1140.0	<0.5	0.98(14)[c]	$E1$
16^-	4615.2	1305.3	<0.5		$E1$
		165.3	<0.5	0.78(16)	$M1$
17^-	4809.2	359.3	<0.5		$E2$
		194.0	<0.5	0.65(7)	$M1$
18^-	5029.5	414.3	<0.5	1.32(13)[c]	$E2$
		220.3	0.7(1)	1.03(12)[c]	$M1$
19^-	5274.6	465.4	<0.5		$E2$
		245.1	0.5(1)	0.81(10)	$M1$

TABLE AI. (*Continued*.)

I_i^π[a]	E_i (keV)[a]	E_γ (keV)[a]	I_γ[b]	R_{DCO}	Assignment
20^-	5544.3	514.8	<0.5		$E2$
		269.7	0.5(1)	0.68(8)	$M1$
21^-	5832.8	558.2	<0.5	1.67(20)[c]	$E2$
		288.5	0.5(1)	0.58(9)	$M1$
22^-	6140.4	596.1	<0.5	0.96(13)	$E2$
		307.6	<0.5	0.69(10)	$M1$
23^-	6460.8	628.0	0.6(1)	1.02(11)	$E2$
		320.4	<0.5	0.62(5)	$M1$
24^-	6794.0	653.6	<0.5	1.02(13)	$E2$
		333.2	<0.5	1.02(10)[c]	$M1$
25^-	7135.9	675.1	<0.5	0.93(10)	$E2$
		341.9	0.5(1)	0.69(7)	$M1$
26^-	7486.7	692.7	<0.5		$E2$
		350.8	<0.5	1.11(15)[c]	$M1$
27^-	7842.3	706.4	0.5(1)	1.07(12)	$E2$
		355.6	<0.5		$M1$
28^-	8208.7	722.0	<0.5		$E2$
		366.4	<0.5		$M1$
29^-	8586.5	744.2	<0.5		$E2$
		377.8	<0.5		$M1$
30^-	8988	779	<0.5		$E2$
		401	<0.5		$M1$
31^-	9386	799	<0.5		$E2$

TABLE AI. (*Continued*.)

I_i^π[a]	E_i (keV)[a]	E_γ (keV)[a]	I_γ[b]	R_{DCO}	Assignment
		Band ED			
25^-	7335.6	770.0	<0.5		$E2$
27^-	8075.1	1387.6	<0.5		$E1$
		739.5	<0.5	0.93(14)	$E2$
29^-	8845.5	807.8	<0.5	0.91(11)	$E2$
		770.4	<0.5	1.10(16)	$E2$
31^-	9661.3	815.8	0.6(1)	0.95(14)	$E2$
33^-	10530.7	869.4	0.5(1)	1.02(7)	$E2$
35^-	11437.4	906.7	0.6(1)	0.93(10)	$E2$
37^-	12384.4	947.0	0.5(1)	1.06(11)	$E2$
39^-	13374.4	990.0	<0.5	1.05(12)	$E2$
41^-	14414.9	1040.5	<0.5	0.98(14)	$E2$
43^-	15512.1	1097.2	<0.5	0.95(13)	$E2$
45^-	16670.1	1158.0	<0.5		$E2$
47^-	17890.9	1220.8	<0.5		$E2$
49^-	19176	1285	<0.5		$E2$

[a] I_i^π, E_i, and E_γ are spin and parity of the depopulated state and the energy of the depopulating γ ray, respectively. The uncertainties in the quoted γ-ray energies are 0.2 keV for most transitions and 0.5 keV for weak transitions (intensity < 1).

[b] Relative intensity (and the error) of the transition with respect to the intensity of 261 keV ($4^+ \rightarrow 2^+$) transition in band G, which has an intensity 100.

[c] DCO ratios obtained by gating on $\Delta I = 1$ transitions. All other DCO ratios are obtained by gating on stretched $E2$ transitions.

[1] A. Bohr and B. R. Mottelson, *Nuclear Structure* (Benjamin, New York, 1975), Vol. II.
[2] S. Ødegård *et al.*, Phys. Rev. Lett. **86**, 5866 (2001).
[3] D. R. Jensen *et al.*, Phys. Rev. Lett. **89**, 142503 (2002), and references therein.
[4] G. Schönwaßer *et al.*, Phys. Lett. **B552**, 9 (2003).
[5] H. Amro *et al.*, Phys. Lett. **B553**, 197 (2003).
[6] P. Bringel *et al.*, Eur. Phys. J. A **24**, 167 (2005).
[7] A. Neußer-Neffgen *et al.*, Phys. Rev. C **73**, 034309 (2006).
[8] Y. C. Zhang *et al.*, Phys. Rev. C **76**, 064321 (2007).
[9] M. K. Djongolov *et al.*, Phys. Lett. **B560**, 24 (2003).
[10] D. J. Hartley *et al.*, Phys. Lett. **B608**, 31 (2005).
[11] D. T. Scholes *et al.*, Phys. Rev. C **70**, 054314 (2004).
[12] R. Bengtsson, www.matfys/lth/se/∼ragnar/ultimate.html.
[13] T. Bengtsson, Nucl. Phys. **A512**, 124 (1990); **A496**, 56 (1989).
[14] H. Amro *et al.*, Phys. Lett. **B506**, 39 (2001).
[15] R. B. Yadav *et al.*, Phys. Rev. C **78**, 044316 (2008).
[16] E. M. Beck *et al.*, Z. Phys. A **327**, 397 (1987).
[17] D. R. Jensen *et al.*, Eur. Phys. J. A **8**, 165 (2000).
[18] I.-Y. Lee *et al.*, Nucl. Phys. **A520**, 641 (1990).
[19] D. C. Radford, Nucl. Instrum. Methods A **361**, 297 (1995).
[20] K. S. Krane, R. M. Steffen, and R. M. Wheeler, Nucl. Data Tables **11**, 351 (1973).
[21] R. B. Firestone *et al.*, *Table of Isotopes* (John Wiley & Sons, New York, 1996).
[22] E. A. McCutchan *et al.*, Phys. Rev. C **76**, 064307 (2007).
[23] E. M. Beck *et al.*, Nucl. Phys. **A464**, 472 (1987).
[24] C.-H. Yu *et al.*, Nucl. Phys. **A511**, 157 (1990).
[25] D. J. Hartley *et al.*, Phys. Rev. C **74**, 054314 (2006).
[26] J. Recht *et al.*, Nucl. Phys. **A440**, 366 (1985).
[27] K. A. Schmidt *et al.*, Eur. Phys. J. A **12**, 15 (2001).
[28] S. Jonsson *et al.*, Nucl. Phys. **A449**, 537 (1986).
[29] D. J. Hartley *et al.*, Phys. Rev. C **72**, 064325 (2005).
[30] D. J. Hartley *et al.*, Phys. Rev. C **80**, 041304(R) (2009).
[31] W. Nazarewicz, M. A. Riley, and J. D. Garrett, Nucl. Phys. **A512**, 61 (1990).
[32] S. Raman *et al.*, At. Data Nucl. Data Tables **36**, 1 (1987).
[33] M. B. Smith *et al.*, Eur. Phys. J. A **6**, 37 (1999).
[34] W. B. Gao *et al.*, Phys. Rev. C **44**, 1380 (1991).
[35] A. Fitzpatrick *et al.*, Nucl. Phys. **A582**, 335 (1995).
[36] F. Dönau, Nucl. Phys. **A471**, 469 (1987).
[37] A. E. Stuchbery *et al.*, Nucl. Phys. **A589**, 222 (1995).
[38] B. E. Chi, Nucl. Phys. **A83**, 97 (1966).
[39] P. M. Walker *et al.*, Phys. Rev. Lett. **65**, 416 (1990).
[40] D. Cullen *et al.*, Phys. Rev. C **52**, 2415 (1995).
[41] P. M. Walker, G. D. Dracoulis, A. P. Byrne, T. Kibèdi, and A. E. Stuchbery, Phys. Rev. C **49**, 1718 (1994).
[42] P. Chowdhury *et al.*, Nucl. Phys. **A485**, 136 (1988).
[43] B. Crowell *et al.*, Phys. Rev. Lett. **72**, 1164 (1994).
[44] C. J. Pearson *et al.*, Phys. Rev. Lett. **79**, 605 (1997).